Space Sci Rev (2020) 216:33
https://doi.org/10.1007/s11214-020-00648-z

IDA4D: Ionospheric Data Assimilation for the ICON Mission

G.S. Bust[1] · **T.J. Immel**[2]

Published online: 19 March 2020

Abstract The Ionospheric Connection Explorer (ICON) mission makes measurements in near-Earth space that provide knowledge of the state of the ionosphere. From the vantage of 575 km altitude in a circular, 27° inclination orbit, it retrieves altitude profiles of the ionospheric density peak in both day and night, characterizing the abundance of oxygen ions in the main ionospheric F-layer. Further, it continuously measures plasma densities and velocities in the immediate vicinity of the observatory. These measurements provide key knowledge required for ICON's investigations and will be regularly provided data products. They also represent an enhancement to a larger set of ionospheric measurements that are regularly obtained by extant networks. The benefit of this enhancement is realized by ingestion of ICON's observations into assimilative models developed to provide a realistic state of the ionospheric plasma density as informed by disparate observations. ICON uses the Ionospheric Data Assimilation Four-Dimensional (IDA4D) model for this task and this report demonstrates the assimilation of simulated ICON ionospheric products into this model. The model captures observations in a 3-dimensional tomographic grid, with a temporal component that maintains "memory" of the observations in particular locales between updates, provided by ICON or other sources. The model therefore provides a unifying framework for viewing ICON measurements as part of an integrated whole-ionospheric assimilation.

Keywords Ionosphere · Data assimilation · Equatorial imaging

1 Introduction

Valid representations of Earth's ionosphere are the goal of numerical modeling efforts that implement tomographic imaging algorithms to assimilate diverse, simultaneous measure-

The Ionospheric Connection Explorer (ICON) mission
Edited by Doug Rowland and Thomas J. Immel

✉ G.S. Bust
gary.bust@jhuapl.edu

[1] Johns Hopkins University Applied Physics Laboratory, Laurel, MD, USA

[2] University of California, Berkeley, USA

ments of this environment. With no dependence on fluid, chemical, or radiative physical simulations, assimilative models of the global ionosphere produce time-evolving three-dimensional (latitude, longitude, altitude) maps of the global electron density distribution solely from observations. These provide a now-cast or reanalysis product whose validity depends on the accuracy of the measurements that are assimilated, as well as the spatial and temporal distribution of the input data. Uniformly accurate imaging of the low-latitude ionosphere has been difficult to achieve due to the paucity of observations, particularly observations that measure the altitude distribution of electron density. As an example, ground-based measurements of vertically integrated total electron content (VTEC) from land-based receiving stations provide no vertical resolution at all, and are limited in geographic distribution (only land-based data). Space-based observations provide key capability, first explored with Faraday rotation from radio beacons (Blumle 1962; Titheridge and Smith 1969; Garriott et al. 1970), and progressing to retrieval of electron density profiles through occultation of GPS satellites (Rocken et al. 1997; Hajj and Romans 1998; Hajj et al. 2000; Lee et al. 2001). Regular occultation samples provided by networks of satellites are an advantageous data source for improving the situation of large data gaps over the oceans, and as proven with COSMIC, will soon be implemented again with COSMIC2 (Yue et al. 2014), simultaneously with the ICON mission.

The goal of this research is to test the ingestion of ICON products in the Ionospheric Data Assimilation Four-Dimensional (IDA4D) (Bust et al. 2004; Bust and Datta-Barua 2014). IDA4D is used for its mature state of development, record of validation and use for various scientific studies as well as civilian and military applications (Mitchell et al. 2017; Datta-Barua et al. 2014; Bust et al. 1994). It has capabilities for assimilating practically all sources of ionospheric measurements, including the ability to assimilate space-based line of sight observations of electron density, ground based TEC observations (Coster and Gaposchkin 1989; Coster et al. 1992; Hajj et al. 1994; Wilson et al. 1995; Hernańdez-Pajares et al. 1998) and parameters retrieved from ionosonde measurements (Breit and Tuve 1925; Appleton and Barnett 1925; Villard 1976). It can directly ingest UV radiances measured in the ionosphere in nighttime, for the fact that these are directly related to the O+ density, the major ion of the F-layer. Further, as we work to ingest simulated ICON data, we test the simultaneous ingestion of simulated COSMIC2 data from its 24° inclination orbit.

The ICON mission (Immel et al. 2017) provides a remarkable view of Earth's space environment at low and middle latitudes, and a new resource for improving our knowledge of the equatorial ionospheric state. In addition to the in-situ observations by an Ion Velocity Meter (IVM) (Heelis et al. 2017), of particular interest for ionospheric imaging are the Far ultraviolet (FUV) observations and the Extreme ultraviolet (EUV) observations. The FUV imager provides 6 simultaneous profiles of 135.6-nm on Earth's limb in nighttime, while also providing imaging of the scene at roughly 4 km resolution (Mende et al. 2017). These data can be directly ingested into IDA4D for the fact that the atmosphere is optically thin to these wavelengths, and the relation of the emissions to the ionospheric source is well understood (Kamalabadi et al. 2018). The EUV imager provides data only in daytime, with height profiles of UV light provided at several wavelengths to support retrieval of the daytime O^+ profiles (Sirk et al. 2017; Stephan et al. 2017). Due to the nonlinear relationship between EUV emissions and O^+ densities, it is the retrieved product that is assimilated.

The U.S. Taiwan FORMOSAT-7/COSMIC 2 mission consists of 6 satellites in a low inclination orbit, taking a variety of ionospheric observations including GNSS radio occultations (RO), topside GNSS slant TEC with positive elevation angles from the LEO satellite receiver to the GNSS satellites, and in-situ ion drifts and electron densities. Each of these three measurements are useful for ionospheric imaging.

The addition of all these data sets to the standard GNSS ground slant TEC measurements and profile observations from ionosondes should provide much improved, more accurate imaging of the low latitude ionosphere. However, the question is how much improvement, how much do each individual type of observations improve the imaging, and finally how much total improvement is there when all instruments are contributing to the imaging algorithms?

For this study, we focus only on observations from ground GNSS TEC, TEC from radio occultations, and FUV from the ICON satellite.

2 Methodology

The goal of this work is to test how the model ingests and utilizes ICON data that will be available after launch. Furthermore, this report describes an investigation of how these data can be combined with other sources to produce a high-fidelity representation of the ionosphere. Here we discuss the skill of the IDA4D model and how the ICON data contribute to its performance.

Before any data are assimilated, the IDA4D model ion densities are seeded with values determined from the IRI (Bilitza 2018). This is the case with every run of the model. To test the assimilation of data, a synthetic dataset is produced for each potential source from a physics-based model run (described below), which is resampled in the same manner as the data from the actual observations will be collected. The data are then ingested at the appropriate locales for individual time-steps of the IDA4D model, as would be done in practice with data that are collected in the field/on orbit.

2.1 Ionosphere Truth Simulation

A Thermosphere Ionosphere Electrodynamic General Circulation Model (TIEGCM) simulation "truth" run of the ionosphere and thermosphere was made for the Memorial Day storm on May 28, 2017. We ran the TIEGCM-ICON with 2.5 × 2.5-degree resolution with 30 second time-step and hourly output. The run was initialed with the solar minimum June Solstice conditions and allowed to freely run. The lower bound wasn't forced with any tides. For high latitude inputs we used the Assimilative Mapping of Ionospheric Electrodynamics (AMIE) data files provided by Atmospheric and Space Technology Associates (ASTRA) for the corresponding days (DOY 147–149). We also feed the model daily F10.7 taken from Natural Resource Canada, F10.7A, and Kp values taken from German Research Center for Geosciences (GFZ).

TIEGCM altitudes end at the exosphere altitude, which is ∼500–600 km. Since the GPS satellites are at ∼20000 km, and a significant fraction of ionosphere density and TEC are above 600 km, the TIEGCM electron density was extended on the topside to 1000 km. The method of extension used was to compute the scale height at the top of the TIEGCM ionosphere using self-consistent TIEGCM neutral temperature and average mass of the neutrals, and then use the scale height with an exponential fall off in altitude to extend the electron density.

In order to accurately simulate the FUV radiances, we need to include the mutual neutralization contribution, which depends on the neutral oxygen. Thus, we extended the neutral oxygen to 1000 km in a manner similar to that of the electron density.

From the ionospheric simulation several data sets were simulated. The simulations were focused on the low-latitude ionosphere, since that is the region that both ICON

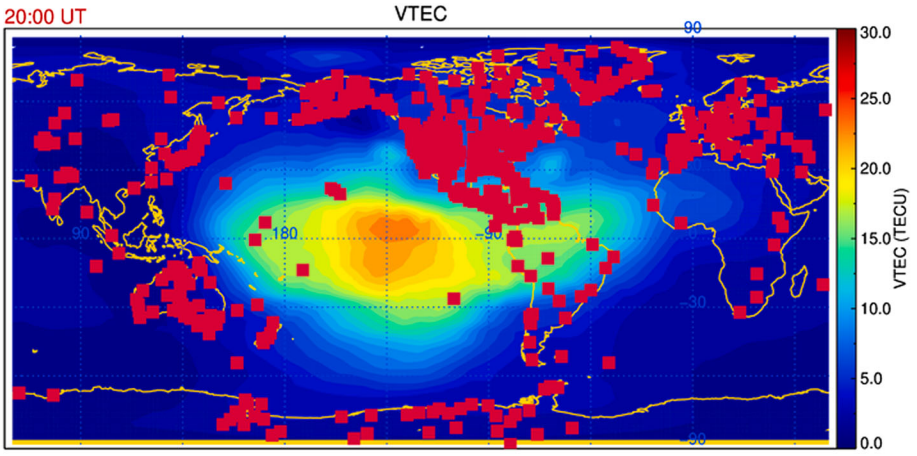

Fig. 1 Coverage of GPS ground stations

and COSMIC-2 will take observations from. The simulated data included ground-based GPS TEC, COSMIC-2 radio occultation TEC, and ICON FUV radiances. The simulation methodology for each of these observations is discussed below.

2.2 Ground-Based GPS TEC

Ground-based GPS slant TEC was simulated using existing low-latitude GPS receiver stations, and actual ephemeris for the GPS satellites. A total of 536 GPS ground stations were used. Figure 1 shows the distribution of GPS ground stations. The ephemeris was taken from IGS SP3 file, slant TEC observations were simulated 2.5 minutes over the entire 24-hour period. For each simulated GPS measurement time, the TIEGCM truth simulations were linearly interpolated in time to the GPS measurement time. The slant path between ground station position and GPS satellite was computed and then divided into 2 km segments. For each segment, the latitude, longitude and altitude along the path was computed, and the TIEGCM electron densities were linearly interpolated onto the measurement position. Finally, the array of electron densities along the path are integrated to produce slant TEC. This is done for every ground GPS station, and every satellite in view (above 15 degrees elevation) throughout the day.

2.3 COSMIC-2 Radio Occultations

Six COSMIC-2 orbits were simulated using 25-degree inclinations and 520 km altitudes. Each simulation began at the equator at 0 UT, and the six orbits were then separated by 72 degrees of longitude.

The COSMIC-2 radio occultation TEC was simulated in a manner similar to the ground GPS. The two primary differences being that the receiver position is now moving along the orbit, and we only simulate for elevation angles that are ≤ 0 (occultations). In addition, we take a measurement every second, restrict the tangent altitudes to be ≥ 80 km, and have only a backward-looking field of view of 140 degrees. As before, this is done for every satellite in view at a given time using the IGS SP3 ephemeris.

2.4 ICON FUV Radiances

Radiances from the FUV optical instrument on the ICON satellite were also simulated for the same TIEGCM "truth" day. The University of California Berkeley (UCB) simulated a realistic ICON orbit using Ephemeris files that assumed a June 2017 launch for ICON out of Kwajalein. The expected 27-degree orbit inclination is assumed and using laboratory measurements of angles on the ICON spacecraft UCB calculated ICON's position, the FUV's field-of-view, the look directions and other necessary quantities at a 12 second cadence for processing upstream.

For each point along the satellite path, the FUV look directions were separated into "limb" observations and "disk" observations, if the tangent altitude is 150 km or less the measurements is defined as disk, otherwise it is limb. For limb radiances, IDA4D expects to have a satellite position and a position at an altitude where no contribution to the radiance is expected, so we extend the look path from the tangent point to 1000 km altitude. We then compute the volume emission rate (VER) at each grid point and time in the TIEGCM truth simulation. We include the mutual neutralization in the VER, using self-consistent neutral oxygen and exosphere temperatures from TIEGCM. Typically, at a given time, the FUV observations on ICON have six "along track" observations for each "across track" direction. However, for this simulation we averaged three look directions together, so that we only have two along track measurements per across track direction. For each FUV observation we then time interpolate VER (taken at 1-hour increments) onto the observation time. We then get the starting and ending positions for the observation and integrate through the VER along the path to compute the radiance.

2.5 ICON EUV Electron Densities

The ICON EUV instrument measures the 617 and 834 nanometer brightness during the day. The observations are ingested into a non-linear radiative transfer model that produces profiles of O^+ density at the tangent point altitudes. Profiles are produced every 12 seconds along the satellite path. At each time, the EUV density profiles a given for 12 different look directions along the satellite path. For this simulation all 12 paths were simulated.

2.6 Analysis Method

The four different data types described above are ingested into IDA4D and inversions of the global electron density field are produced. The temporal update in IDA4D is chosen to be five-minute increments. The latitudinal resolution was 4 degrees, while the longitudinal resolution 10 degrees of great circle distance at the equator, or $\sim$1100 km. Since the longitude is not a regular array the latitudes and longitudes are represented as a 1-dimensional array of 2-tuples points (latitude, longitude). Figure 2 shows the latitude-longitude grid on a Mercator projection of the globe. There are 143 altitude grid points ranging from 92.5 km to 1475 km. From 92.5 km to 600 km the altitude resolution is 5 km. From 600–800 km it is 10 km, from 800–1000 km it is 20 km and from 1000 to the top of the grid it is 50 km resolution.

Figure 3 presents an IDA4D inversion for the case of ingesting ground GPS TEC and radio occultations from the COSMIC-2 mission. The top figure is the vertical TEC map for the truth TIEGCM run. The middle plot is the International Reference Ionosphere (IRI) which is the background model used to initiate the IDA4D inversion. Note that the colorbar range is 40 TECU which is twice the range of the truth image. Thus, the background model

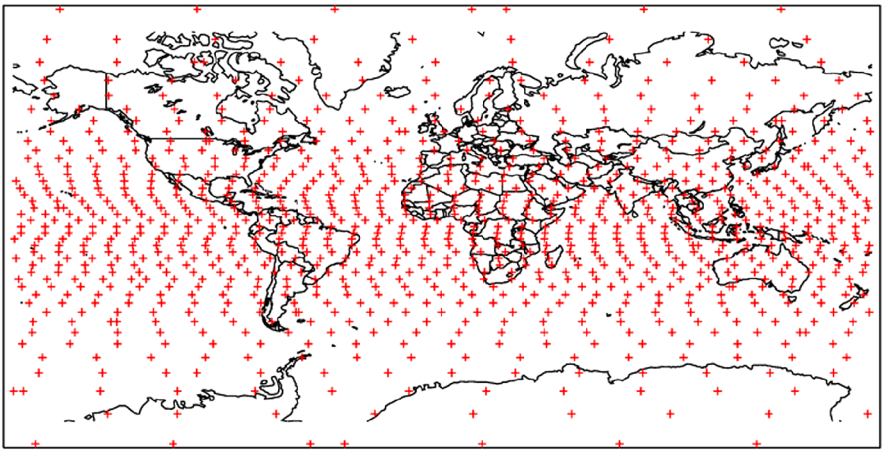

Fig. 2 Example of IDA4D two-dimensional horizontal irregular grid

IDA4D starts from has much higher density than the truth, and shows a clear latitudinal separation between the two equatorial anomalies that the truth does not show. The lower plot is the IDA4D reconstruction. The densities are much closer to the truth than the initial IRI model densities, and the overall horizontal structure of the equatorial region is now much closer to the truth.

The IDA4D inversions are run for a full day, with results saved every 5 minutes. Several different runs were made with different combinations of the four data sets described above. The different combinations of IDA4D runs were: (1) FUV only data, (2) EUV only data, (3) ground GPS only data, (4) Radio occultation data only, and (5) GPS and RO data. Each of the runs had the same exact grid, IRI model, and model covariances.

3 Results

3.1 FUV Analysis

3.1.1 Example FUV Profiles

Below are two sets of comparison profiles for the FUV only ingested data case. The black squares represent the simulated truth, while the horizontal black dashes represent the errors on the data. The errors would normally consist of the actual data errors (Poisson counting), and representation error. For this study the representation error was 10% of the radiance, and the minimum error was set at 5 Rayleighs (R). The first two plots are for very early in the assimilation run, at approximately 1 UT and at mid-latitudes. The plot altitudes are taken at tangent latitude and longitudes. For this case, the radiances are quite small, so that the minimal error of 5R is as large as the data. Regardless, Fig. 4 shows that the IDA4D estimation of the radiances (blue circles) is very close to the truth, even though the original model estimate from IRI is very poor (red diamonds). This demonstrates IDA4D is able to adjust densities to accurately fit even small radiances with large errors.

However, even with an almost perfect fit, Fig. 5 shows that the IDA4D estimated electron density profile does not exactly match the truth. While the maximum electron density is well estimated, ∼1/2 of the IRI model, the peak height is too low, below about 300 km, the

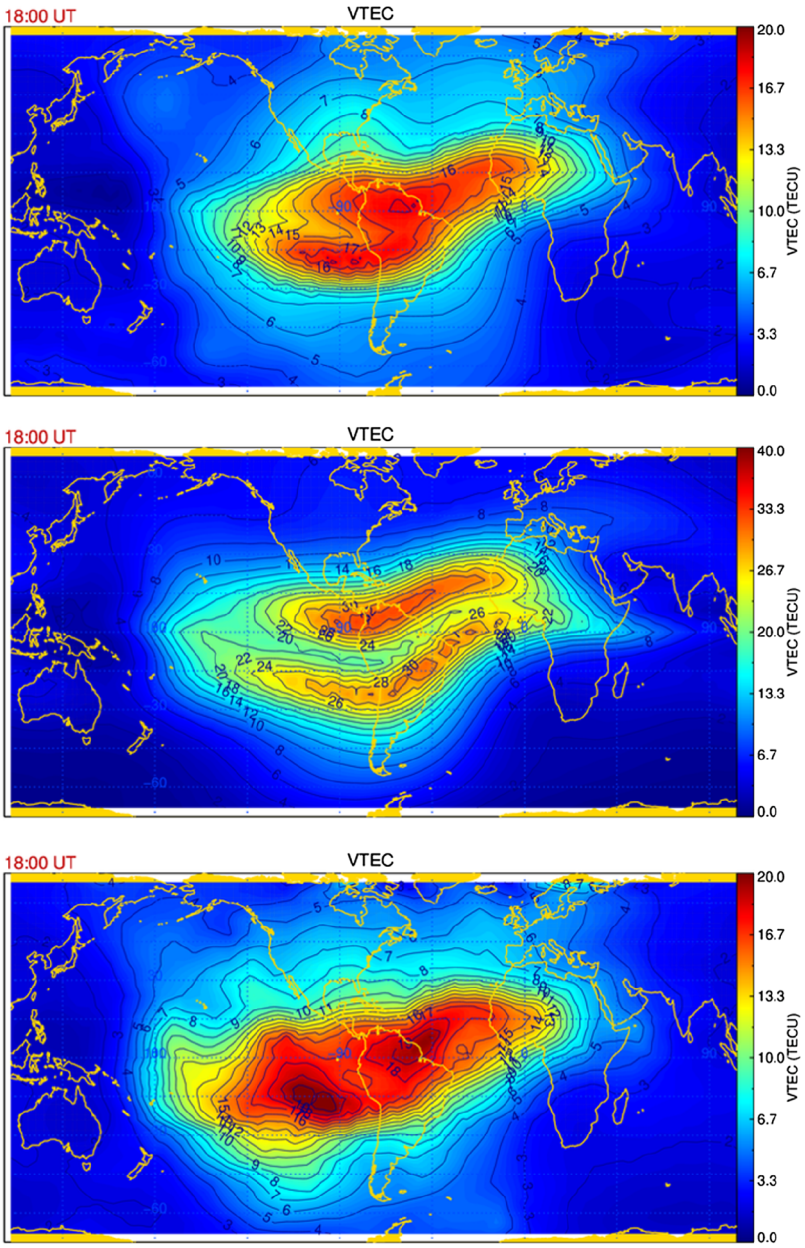

Fig. 3 Example IDA results taken at 18 UT. The top plot is. The TIEGCM truth, the middle plot is the IRI model background to IDA4D and the lower plot is the IDA4D reconstruction

analyzed (formal errors) from IDA4D are too small to include the truth. What this represents that a single profile of radiances does not provide a unique inversion. This is of course due to the fact that the measured radiances represent the integration over a large spatial region along the look direction, where there are gradients and variability in the electron

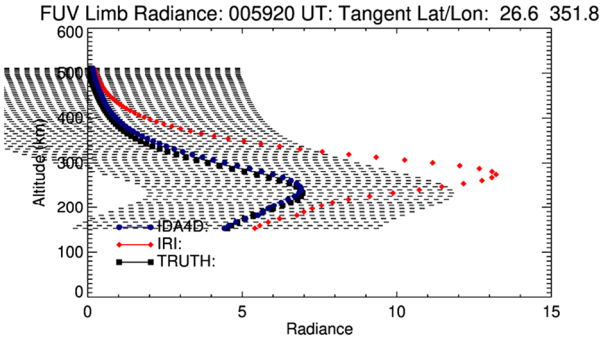

Fig. 4 Example plot at 59 minutes, 20 seconds UT of simulated "truth" Radiances, with simulated error bars in black, initial model prediction from IRI in red, and IDA4D estimation of the truth in blue

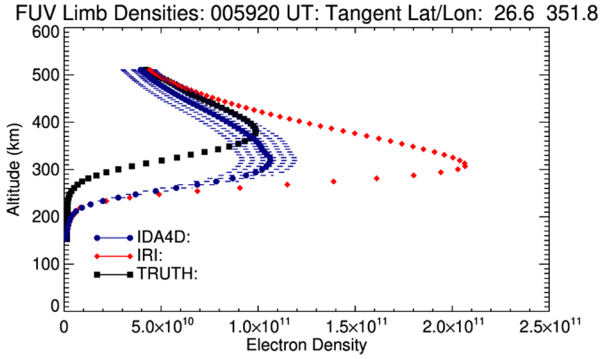

Fig. 5 Truth electron density profile at the tangent latitude and longitude (black) from Fig. 4 truth radiances. IDA4D estimates of electron density given in blue filled circles along with analyzed errors, and the initial model, IRI in red diamonds

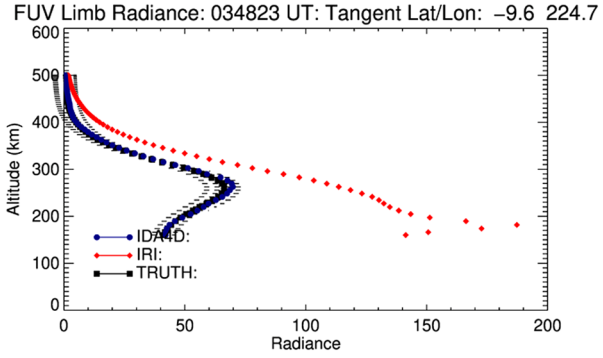

Fig. 6 Similar to Fig. 4, only later in the day (03:48 UT) and at a lower latitude (−9.6 degrees)

density distribution. A single set of measurements versus tangent altitudes does not carry enough information to uniquely adjust the densities in both altitude and horizontally along the look direction. Either one needs additional measurements from ground GPS TEC and/or radio occultation (RO) TEC to more uniquely specify the electron density field, or a better initial forecast of the background density field, particularly its horizontal gradients. This case was early in the day. The Kalman filter, which allows information from earlier times to be propagated forward, had not had enough time to be effective, so the initial forecast ionosphere was primarily IRI.

Figures 6 and 7 are taken a bit later in the day a bit later in the day at about 03:48 UT, and at equatorial latitudes. Now the truth radiances are much larger ∼50 Rayleighs, and the

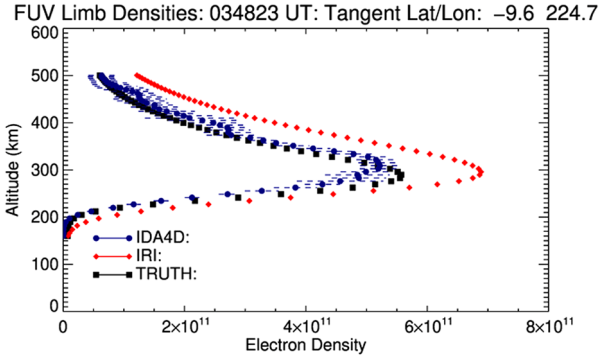

Fig. 7 The same as Fig. 5, but for the radiances in Fig. 6

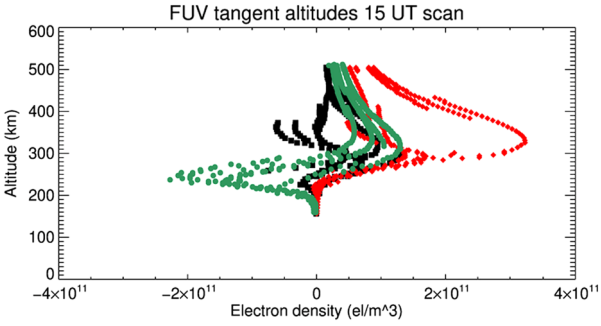

Fig. 8 Profile comparisons at 15 UT along an FUV limb scan. Black squares are FUV only IDA4D—TIEGCM truth, while green circles are GPS only—TIEGCM truth and red diamonds are IRI—TIEGCM truth

errors are a much smaller fraction. Still, even though the IRI model prediction is too large by a factor of 4, IDA4D fits the truth within error bars, for the entire profile.

Figure 7 shows the reconstructed profiles at the tangent altitudes of the measured radiances in Fig. 6. Now, the IDA4D estimate of electron density is much closer to the truth. The peak altitude from IDA4D is ∼30 km too high, and the peak density ∼4E10 too low, but overall a very good fit. It is likely that 3+ hours of satellite passes, and IDA4D estimations every 5 minutes has pre-conditioned the ionosphere to be closer to the true ionosphere, and therefore allowed the inversion to produce more accurate profiles.

3.1.2 Comparisons of Profiles Along ICON FUV Limb Scans

The above was an example of the type of results we obtained. To do a statistical analysis, we take all the cases for when we had FUV profiles for the full day, and compare the IDA4D estimation of electron density profiles at the tangent altitudes, with the truth. This should represent a kind of "best" result. For comparison purposes we also take profiles from the background model IRI, and profiles from an IDA4D run with only ground GPS data ingested. Figure 8 shows an example set of profiles from an FUV limb scan at 15 UT. The reconstructed electron density profiles are taken at the tangent points of the limb scans as a function of altitude. The black squares represent the difference between the IDA4D reconstructions and the simulated TIEGCM "truth" for this case. The red diamonds are for the difference between the IRI empirical model that serves as the background for IDA4D, and truth. The green filled circles give the difference between the case where only ground slant TEC from GPS data is assimilated into IDA4D and the truth.

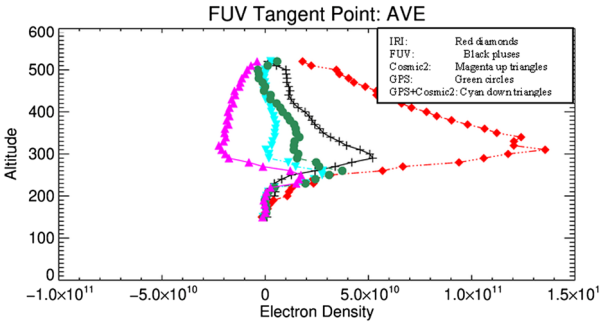

Fig. 9 Average difference between the TIEGCM truth electron densities and IRI, IDA4D-FUV, IDA4D-COSMIC-2, IDA4D-GPS, IDA4D-GPS-COSMIC2 electron densities as a function of altitude

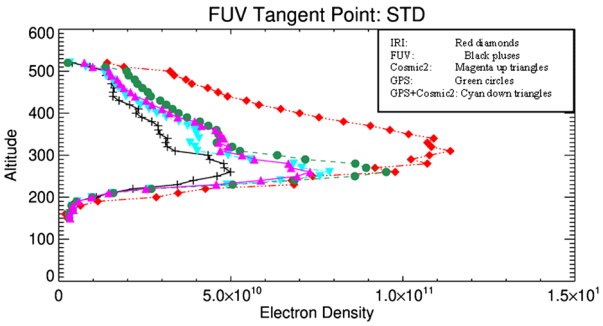

Fig. 10 The same as for Fig. 9, except now for the standard deviation rather than the average difference

The difference between the IDA4D estimated densities and the truth (black) is less than $\pm$1E11 el/m^3 at all altitudes, and less than $\pm$5E10 and lower and higher altitudes. The GPS only IDA4D results are similar to FUV IDA4D results at higher altitudes, somewhat worse at ~300–400 km altitudes, and much worse (and negatively biased) at lower altitudes. In fact, compared to the initial model IRI, the GPS only solution is worse than the initial model at lower altitudes. This suggests the importance of combining ground GPS with FUV profile measurements. The deviation from the truth for background IRI model (red) much larger than from the reconstructed IDA4D (black), and is always positively biased.

Figures 9 and 10 represent the statistics of comparing the various IDA4D reconstructions described above, against the TIEGCM "truth". For 24 hours over the day, for all the cases throughout the day, when there were ICON FUV limb scans, the lines of sight for each FUV measurement were extracted, and the and tangent points (latitude, longitude, altitude) were computed. The tangent altitudes were binned into 10 km regions from 150 km to 520 km altitude and all of the reconstructed electron densities for each tangent latitude and longitude were collected into the altitude bins. This was done for the truth and for the FUV, GPS, COSMIC-2, and GPS+COSMIC-2 IDA4D reconstructions, as well as for the background IRI model. The average difference and standard deviation between truth and reconstruction was then computed for each height bin. Figure 9 presents the average difference between the truth, and the various IDA4D reconstructions as a function of altitude, while Fig. 10 presents the standard deviation of the difference as a function of altitude.

3.2 EUV Analysis

For the EUV analysis, IDA4D ingested the tangent profiles of electron density, simulated from the TIEGCM truth, for each of the twelve profile directions at each time. Analysis

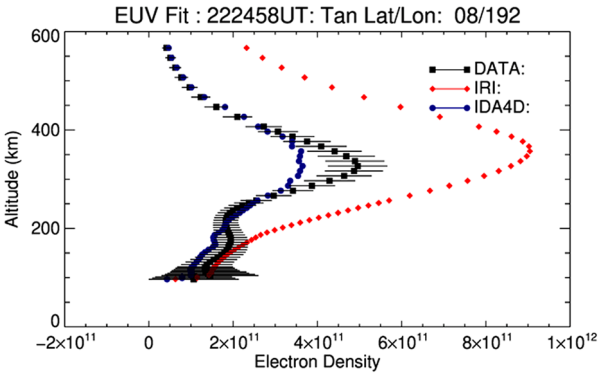

Fig. 11 Example plot at 22 hours, 24 minutes, 58 seconds UT, at a longitude of 192 and latitude of 8 degrees of simulated "truth" retrieved EUV electron densities, with simulated error bars in black, initial model prediction from IRI in red, and IDA4D estimation of the truth in blue

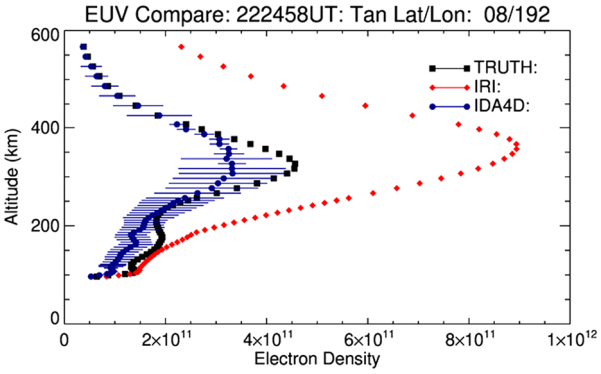

Fig. 12 Truth electron density profile at the tangent latitude and longitude (black) from the

similar to that carried out for the FUV simulations is presented below. The biggest differences being IDA4D is directly ingesting derived electron density profiles from the EUV data.

3.2.1 Example EUV Profiles

Below Figs. 11–14 present example results from the entire day of EUV IDA4D estimations. All figures are taken for the same time, 22:24:58 UT. Figures 11 and 12 are taken for the 12th look direction, 192 degrees longitude and 8 degrees latitude, while Figs. 13–14 are taken for the 1st look direction 177 degrees longitude and 16 degrees latitude. The two look directions are significantly separate in geophysical position.. For all Figures, the initial model IRI is significantly too large. Comparing Figs. 11 and 13 shows that the true ingested data (black squares) is quite different for the two look directions. For Fig. 13, the IDA4D estimation fits the data within error. However, in Fig. 11, the IDA4D estimation is outside of error bars for ∼300–400 km altitudes. This may indicate that the longitudinal correlation used (10 degrees of geomagnetic longitude) is too large to allow IDA4D to fit both observations. Similarly, for Fig. 14, the IDA4D estimation of "truth" is within analyzed error bars for almost all altitudes. However, Fig. 12 shows that IDA4D is a bit outside analyzed error for the same 300–400 km altitude range. One take-away may be that IDA4D needs to be "tuned" in terms of its horizontal model error correlations for ICON FUV and EUV data to better pick up the variabilities observed in the data.

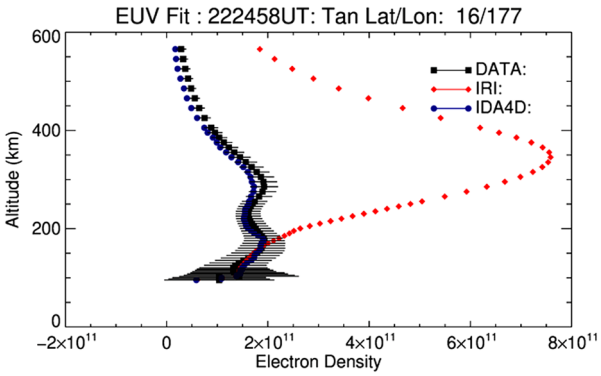

Fig. 13 The same as Fig. 11, except for a longitude of 177 degrees and latitude of 16 degrees

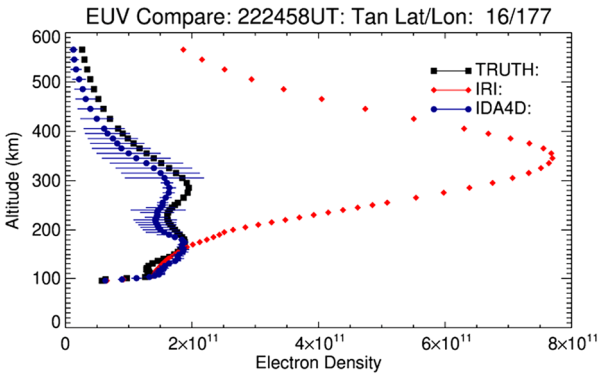

Fig. 14 Same as Fig. 12, except for a longitude of 177 degrees and latitude of 16 degrees

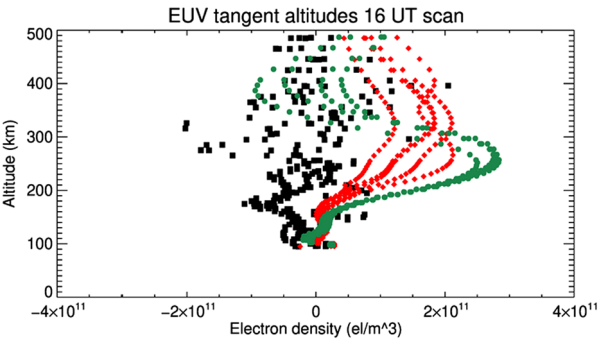

Fig. 15 Profile comparisons at 16 UT along an EUV observation. Black squares are EUV only IDA4D—TIEGCM truth, while green circles are GPS only—TIEGCM truth and red diamonds are IRI—TIEGCM truth

3.2.2 Comparisons of ICON EUV Profiles

The above was an example of the type of results we obtained. To do a statistical analysis, we perform a similar analysis as we did for the EUV case. We take all the cases for when we had EUV profiles for the full day, and compare the IDA4D estimation of electron density profiles at the tangent altitudes, with the truth. This should represent a kind of "best" result. For comparison purposes we also take profiles from the background model IRI, and profiles from an IDA4D run with only ground GPS data ingested. Figure 15 shows an example set of profiles from an EUV limb scan at 16 UT. The reconstructed electron density profiles

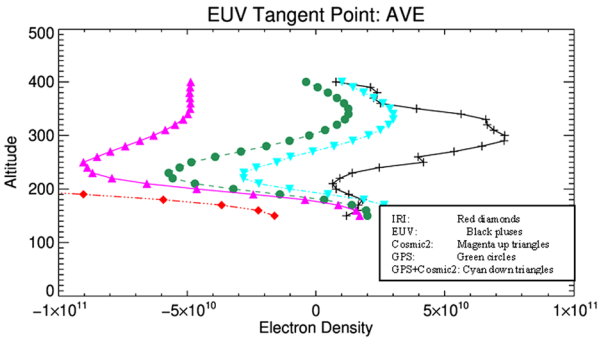

Fig. 16 Average difference between the TIEGCM truth electron densities and IRI, IDA4D-EUV, IDA4D-COSMIC-2, IDA4D-GPS, IDA4D-GPS-COSMIC2 electron densities as a function of altitude

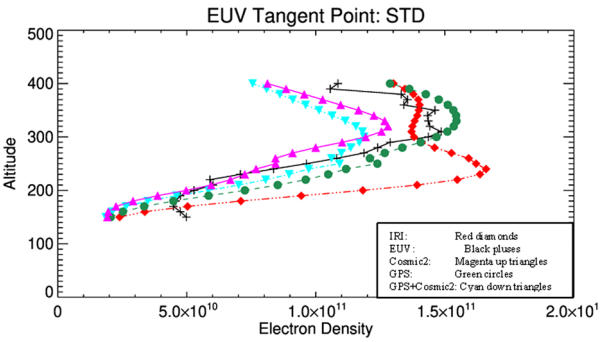

Fig. 17 The same as for Fig. 16, except now for the standard deviation rather than the average difference

are taken at the tangent points of the EUV tangent profiles as a function of altitude. The black squares represent the difference between the IDA4D reconstructions and the simulated TIEGCM "truth" for this case. The red diamonds are for the difference between the IRI empirical model that serves as the background for IDA4D, and truth. The green filled circles give the difference between the case where only ground slant TEC from GPS data is assimilated into IDA4D and the truth.

The difference between the IDA4D estimated densities and the truth (black) is less than $\pm$1E11 el/m^3 at all altitudes, except for a few points around 250–300 km altitudes, and less than $\pm$5E10 and lower and higher altitudes. The GPS only IDA4D results are similar to much worse than the EUV IDA4D results in the range of $\sim$150–400 km altitudes, and are in fact positively biased and worse than IRI. The deviation from the truth for background IRI model (red) worse than IDA4D for the $\sim$200–400 km range, but is somewhat better at the lowest altitudes.

Figures 16 and 17 represent the statistics of comparing the various IDA4D reconstructions described above, against the TIEGCM "truth". For 24 hours over the day, for all the cases throughout the day time, when there were ICON EUV profiles. For each EUV profile latitude and longitude, the altitudes were binned into 10 km regions from 150 km to 520 km altitude and all of the reconstructed electron densities for each profile latitude and longitude were collected into the altitude bins. This was done for the truth and for the EUV, GPS, COSMIC-2, and GPS+COSMIC-2 IDA4D reconstructions, as well as for the background IRI model. The average difference and standard deviation between truth and reconstruction was then computed for each height bin. Figure 16 presents the average difference between the truth, and the various IDA4D reconstructions as a function of altitude, while Fig. 17 presents the standard deviation as a function of altitude.

Table 1 Skill score comparisons

IDA4D case	FUV tangent profiles	EUV tangent profiles
FUV	0.62	N/A
EUV	N/A	0.46
GPS	0.53	0.42
COSMIC2	0.59	0.50
GPS + COSMIC2	0.62	0.56

3.3 Skill Scores

The previous analysis has looked at the comparisons visually and statistically. We can also investigate analytically using skill scores. For this analysis we define the skill score as:

$$S = 1 - \frac{[\langle (I-T)^2 \rangle]^{\frac{1}{2}}}{[\langle (M-T)^2 \rangle]^{\frac{1}{2}}}$$

where I is the IDA4D reconstruction data, T is the truth data and M is the IRI model data. The brackets indicate take an average. Thus, the skill is given by taking the ratio of the RMS error between IDA4D and Truth, and IRI and Truth, and then subtracting from 1. Note that if the IDA4D estimation matches truth exactly, the skill is 1. If, on average, it is no better than the model the skill goes to zero, and if it is worse than the model, the skill is negative. Table 1 gives the skill scores for the FUV tangent profiles described above and the EUV profiles, for the different data sets.

4 Discussion/Summary

We have demonstrated the utility of ingesting ICON FUV and EUV only data into IDA4D. For the FUV case, Figs. 4 and 6 have shown that IDA4D is able to accurately fit and reproduce the ingested radiances within error bars. However, while the IDA4D inversions from Fig. 7 are close to the true ionosphere, those from Fig. 5 do not match the truth that closely. This result demonstrates that for integrated measurements even a good fit, within error bars does not necessarily produce a unique solution. For the EUV case, Figs. 11 and 13 show two case "fits" that are at the same time, but separated in along track look direction by 15 degrees of longitude. Figure 11 does not show a good fit to the data, while Fig. 13 does. Similarly, Fig. 12 shows the IDA4D reconstruction is not a good fit to the true ionosphere, while Fig. 14 is. This result demonstrates that the data (and therefore true ionosphere) has a significant amount of ionospheric variability over a small spatial region, and that the same global 3D IDA4D inversion does not accurately capture that variability, even with good observations. This suggests that the standard "out of the box" IDA4D is not optimized for ICON data. ICON is unique in the amount of spatial observations along satellite track it continually makes. IDA4D needs to be "tuned" in terms of the spatial error correlations and spatial resolution of the grid, both of which are user input parameters.

The statistical results of the FUV case are presented in Figs. 9 and 10. The standard deviation errors in Fig. 10 for the ICON FUV only IDA4D reconstructions (black plusses) are surprisingly good, with the errors less than $\sim$ 5E10 el/m^3 at all altitudes, and less than $\sim$ 1E10 for altitudes above 400 km and below 200 km. These are significantly smaller than any of the other IDA4D estimations. The COSMIC2 alone, and the GPS+COSMIC2 are roughly

equivalent, but have significantly bigger standard deviations than the FUV estimations for all altitudes above ∼220 km. The average errors in Fig. 9, paint a slightly different story from the standard deviations. In fact, the average errors for the FUV IDA4D is very similar to the standard deviation errors, with the averages errors biased positively. The IRI errors are also biased positively and are quite large. The GPS average errors are actually smaller than the FUV in the main F-region of the ionosphere, and are only slightly positive biased, becoming negatively biased at higher altitudes. Interestingly, the COSMIC2 IDA4D inversions are biased negatively almost as the FUV are biased positively. Finally, the best average errors seem to be due to using both GPS and COSMIC2 together. There are several possible reasons for the improved average errors from GPS (and then COSMIC2 with GPS). First, it could be the large number of GPS stations and observations. Which, since it is slant TEC, might not pick up all the statistical variability with altitude, might produce good results—*on average!!* The second factor could be a mutual neutralization effect. IDA4D uses MSIS to compute the mutual neutralization term. The TIEGCM truth simulation, uses its own self-consistent modeling of the neutrals. It is possible that there is an inherent bias between MSIS and TIEGCM neutrals. Regardless, the two results, average and standard deviation errors, when taken together, imply that the most accurate IDA4D inversions might come from combining FUV, ground GPS and COSMIC2 all together—which, in fact, is exactly what is intended once we are collecting data from ICON.

The standard deviation errors in Fig. 17 for the ICON EUV only IDA4D reconstructions (black plusses) have a maximum error $\sim$ 1.5E11 el/m^3 a F2 peak altitude of ∼300 km, then dropping to under $1.0E11$ el/m^3 at ∼220 km and below. For daytime electron densities, which can be as high as 1E12 el/m^3 or higher, these are quite good results. The GPS only IDA4D estimation is worse than the EUV retrievals at all altitudes, which is expected. The COSMIC2 alone, and the GPS+COSMIC2 are roughly equivalent, and are somewhat better than the EUV IDA4D estimates at most altitudes. This is somewhat surprising, since in principle we are estimating electron densities at the locations of the data. However, this most likely indicates the importance of spending some effort tuning both the grid and the error covariances for ICON observations, which are a unique data set. The average errors in Fig. 16, demonstrate a different aspect of the IDA4D inversions. The EUV only inversions are positively biased at all altitudes, with the maximum error $\sim$ 0.75E10 el/m^3 at 300 km altitude. However, the GPS, COSMIC2 and the both together, all are negatively biases for F region altitudes and then slightly positively biased at high and low altitudes. It is useful to note that these biases are small compared to the standard deviations, just a few percent at most altitudes. Since the GPS and COSMIC2 data together, improved the average errors, it is expected that if EUV is added as an additional data source, the average errors will get smaller, which again as was for the FUV case, is exactly what is intended once we are collecting data from ICON.

Finally, the results can also be interpreted in terms of the skill scores in Table 1 for the FUV and EUV analysis. The IDA4D estimation with only FUV data produced a skill score of 0.62, which is quite good. One would hope this would be the case, since we are looking at tangent profiles along the FUV look directions, but considering gradients and all the other issues, it is still a very good result, and better than either the ground GPS alone (0.53) or the COSMIC2 alone (0.59). However, the combined GPS and COSMIC2 produce the same skill score as the FUV alone, again indicating that using all three data sets will produce the most accurate results.

For the EUV, the situation is more complicated. The EUV skill score of 0.46 is better than GPS (0.42), but not as good as COSMIC2 (0.50) or GPS and COSMIC2 together (0.56). This is clearly due to the fact that the IDA4D grid and error covariances are such that the

high spatial resolution EUV data is inconsistent in regions of high spatial variability, and forcing IDA4D to either produce incorrect "average" results from the data, or produce good results at one spatial point and poor results at another spatial point—all within the same 3D inversion at a given time. With both GPS and COSMIC2 there is no such data inconsistency, since the ingested data is at a much lower spatial resolution. This is an important point, since it suggests that optimizing IDA4D for ICON, will take advantage of the high spatial resolution observations, and produce more accurate high-resolution 3D maps of electron densities that dynamically adjust over time.

Future work will focus on optimizing IDA4D for the ICON observational data sets. As such, this initial simulation result can serve as a baseline, particularly the skill scores to help assess the best set of parameters for IDA4D to make the best optimal use of ICON observations.

References

E.V. Appleton, M.A.F. Barnett, Local reflection of wireless waves from the upper atmosphere. Nature (London) **115**, 333–334 (1925)

D. Bilitza, IRI the international standard for the ionosphere. Adv. Radio Sci. **16**, 1–11 (2018). https://doi.org/10.5194/ars-16-1-2018

L.J. Blumle, Satellite observations of the equatorial ionosphere. J. Geophys. Res. **67**, 4601 (1962)

G. Breit, M.A. Tuve, A radio method of estimating the height of the conducting layer. Nature (London) **116**, 357 (1925)

G.S. Bust, S. Datta-Barua, Scientific investigations using IDA4D and EMPIRE, in *Modeling the Ionosphere-Thermosphere System*, ed. by J. Huba, R. Schunk, G. Khazanov (Wiley, Chichester, 2014). https://doi.org/10.1002/9781118704417.ch23

G. Bust, J.A. Cook, G.R. Kronschnabl, C.J. Vasicek, S.B. Ward, Application of ionospheric tomography to single-site location range estimation. Int. J. Imaging Syst. Technol. **5**, 160–168 (1994)

G.S. Bust, T.W. Garner, T.L. Gaussiran II., Ionospheric data assimilation three dimensional (IDA3D): a global, multi-sensor, electron density specification algorithm. J. Geophys. Res. **109**, A11312 (2004). https://doi.org/10.1029/2003JA010234

A.J. Coster, E.M. Gaposchkin, Use of GPS pseudo-range and phase data for measurement of ionospheric and tropospheric refraction, in *Institute of Navigation Satellite Division, International Technical Meeting, 2nd, Proceedings (A90-43676 19-17)*, Colorado Springs, CO, Sept 27–29, 1989 (Institute of Navigation, Washington, 1989), pp. 439–443

A.J. Coster, E.M. Gaposchkin, L.E. Thornton, Real-time ionospheric monitoring system using GPS. Navigation **39**, 191–204 (1992). https://doi.org/10.1002/j.2161-4296.1992.tb01874.x

S. Datta-Barua, T. Walter, G.S. Bust, W. Wanner, Effects of solar cycle 24 activity on WAAS navigation. Space Weather **12**, 46–63 (2014). https://doi.org/10.1002/2013SW000982

O.K. Garriott, A.V. DaRosa, W.J. Ross, Electron content obtained from Faraday rotation and phase path length variations. J. Atmos. Terr. Phys. **32**, 705 (1970)

G.A. Hajj, L.J. Romans, Ionospheric electron density profiles obtained with the global positioning system: results from the GPS/MET experiment. Radio Sci. **33**, 175–190 (1998)

G.A. Hajj, R. Ibanezmeier, E.R. Kursinski, L.J. Romans, Imaging the ionosphere with the global positioning system. Int. J. Imaging Syst. Technol. **5**, 174–184 (1994)

G.A. Hajj, L.C. Lee, X. Pi, L.J. Romans, W.S. Schreiner, P.R. Straus, C. Wang, COSMIC GPS ionospheric sensing and space weather. Terr. Atmos. Ocean. Sci. **11**, 235–272 (2000)

R.A. Heelis, R.A. Stoneback, M.D. Perdue et al., Ion velocity measurements for the ionospheric connections explorer. Space Sci. Rev. **212**, 615–629 (2017). https://doi.org/10.1007/s11214-017-0383-3

M. Hernańdez-Pajares, J.M. Juan, J. Sanz, J.G. Sole, Global observation of the ionospheric electronic response to solar events using ground and LEO GPS data. J. Geophys. Res. **103**, 20789–20796 (1998)

T.J. Immel, S.L. England, S.B. Mende, R.A. Heelis, C.R. Englert, J. Edelstein, H.U. Frey, E.J. Korpela, E.R. Taylor, W.W. Craig, S.E. Harris, M. Bester, G.S. Bust, G. Crowley, J.M. Forbes, J.-C.G. erard, H.M. Harlander, J.D. Huba, B. Hubert, F. Kamalabadi, J.J. Makela, A.I. Maute, R.R. Meier, C. Raftery, P. Rochus, O.H.W. Siegmund, A.W. Stephan, G.R. Swenson, S. Frey, D.L. Hysell, A. Saito, K.A. Rider, M.M. Sirk, The ionospheric connection explorer mission: mission goals and design. Space Sci. Rev. (2017). https://doi.org/10.1007/s11214-017-0449-2

F. Kamalabadi, J. Qin, B. Harding, D. Iliou, J. Makela, R.R. Meier, S.L. England, H.U. Frey, S.B. Mende, T.J. Immel, Inferring nighttime ionospheric parameters with the far ultraviolet imager onboard the ionospheric connection explorer. Space Sci. Rev. **214**, 70 (2018)

L.-C. Lee, C. Rocken, E.R. Kursinski (eds.), *Applications of Constellation Observing System for Meteorology, Ionosphere and Climate* (Springer, New York, 2001). 384 pp.

S.B. Mende, H.U. Frey, K. Rider, C. Chou, S.E. Harris, O.H.W. Siegmund, S.L. England, C.W. Wilkins, W.W. Craig, P. Turin, N. Darling, T.J. Immel, J. Loicq, P. Blain, E. Syrstadt, B. Thompson, R. Burt, J. Champagne, P. Sevilla, S. Ellis, The far ultra-violet imager on the ICON mission. Space Sci. Rev. (2017). https://doi.org/10.1007/s11214-017-0386-0

C.N. Mitchell, N.R. Rankov, G.S. Bust, E. Miller, T. Gaussiran, R. Calfas, J.D. Doyle, L.J. Teig, J.L. Werth, I. Dekine, Ionospheric data assimilation applied to HF geolocation in the presence of traveling ionospheric disturbances. Radio Sci. **52**, 829–840 (2017). https://doi.org/10.1002/2016RS006187

C. Rocken et al., Analysis and validation of GPS/MET data in the neutral atmosphere. J. Geophys. Res. **102**, 29849–29966 (1997)

M.M. Sirk, E.J. Korpela, Y. Ishikawa, J. Edelstein, E.H. Wishnow, C. Smith, J. McCauley, J.B. McPhate, J. Curtis, T. Curtis, S.R. Gibson, S. Jelinsky, J.A. Lynn, M. Marckwordt, N. Miller, M. Raffanti, W. Van Shourt, A.W. Stephan, T.J. Immel, Design and performance of the ICON EUV spectrograph. Space Sci. Rev. (2017). https://doi.org/10.1007/s11214-017-0384-2

A.W. Stephan, E.J. Korpela, M.M. Sirk, S.L. England, T.J. Immel, Daytime ionosphere retrieval algorithm for the ionospheric connection explorer (ICON). Space Sci. Rev. (2017). https://doi.org/10.1007/s11214-017-0385-1

J.E. Titheridge, W.D. Smith, The electron content of the low latitude ionosphere. Planet. Space Sci. **17**, 1667 (1969)

O.G. Villard, The ionospheric sounder and its place in the history of radio science. Radio Sci. **11**(11), 847–860 (1976). https://doi.org/10.1029/RS011i011p00847

B.D. Wilson, A.J. Mannucci, C.D. Edwards, Subdaily northern hemisphere ionospheric maps using an extensive network of GPS receivers. Radio Sci. **30**, 639–648 (1995)

X. Yue, W.S. Schreiner, N. Pedatella, R.A. Anthes, A.J. Mannucci, P.R. Straus, J.-Y. Liu, Space weather observations by GNSS radio occultation: from FORMOSAT-3/COSMIC to FORMOSAT-7/COSMIC-2. Space Weather **12**, 616–621 (2014). https://doi.org/10.1002/2014SW001133